

Joule heating estimation of photovoltaic module through cells temperature measurement

Erkata Yandri¹, Naoto Hagino²

¹Graduate School of Renewable Energy, Darma Persada University, East Jakarta, Indonesia

²Department of Mechanical Engineering, Faculty of Engineering, Kanagawa Institute of Technology, Atsugi, Japan

Article Info

Article history:

Received Jul 25, 2021

Revised Mar 25, 2022

Accepted Apr 10, 2022

Keywords:

Continuous probability

PV efficiency

PV temperature

Series resistance loss

Thermal distribution

Thermal efficiency

ABSTRACT

Module temperature has a role in determining a PV module's performance. The purpose of this paper is to estimate the Joule heating in a photovoltaic (PV) module by comparing during PV-On (electricity generation) and PV-Off (without electricity generation). Joule heating was less evaluated due to simplifying formulation, which is easier to implement in experimental observation as proposed in this work. The experiment collected the temperature distributions of the PV module during PV-On and PV-Off. PV module temperature distribution follows the normal distribution curve as the irradiation uniformity pattern of the solar simulator has a slight ≤ 0.3 °C difference between PV-On and PV-Off. Joule heating slightly increased the PV module temperature by 0.53 K/A, proportional to the irradiances. Joule heating has increased almost seven times from 2.65 W at 700 W/m² to 18.07 W at 1000 W/m². Joule heating might slightly increase the overall thermal conductivity and slightly decrease the thermal resistances. It might affect the heat transfer. This research may improve the procedures prediction of PV or photovoltaic-thermal (PVT) collector temperature by considering Joule heating.

This is an open access article under the [CC BY-SA](#) license.



Corresponding Author:

Erkata Yandri

Graduate School of Renewable Energy, Darma Persada University

Radin Inten 2 St., Pondok Kelapa, East Jakarta 13450, Indonesia

Email: erkata@gmail.com, erkata@pasca.unsada.ac.id

1. INTRODUCTION

The sun is an abundant source of energy available on earth. Based on the latest research, conversion of solar energy into electricity can reach 24% efficiency using mono-crystalline silicon (mc-Si) of photovoltaic (PV) modules [1] and into thermal energy by 70% efficiency using water-based flat-plate thermal collectors [2]. The rest of the unused solar energy is reflected or becomes heat lost by convection. Theoretically, PV module performance decreases with increasing module temperature or vice versa [3], [4]. For performance stability, converting heat into valuable energy can control the PV module temperature. That is one of the reasons for combining a PV module with a thermal collector into a hybrid photovoltaic-thermal (PVT) collector [5]. The conversion of solar energy is up to 80-90% [6]. The performance of the PV module and thermal collector influence the total performance of the PVT collector [7].

Here, PV temperature has a role in determining optimal performance. Many researchers evaluated the PV module or PVT collector performance for a long time. The actual measured PV temperature is the effect of irradiance and Joule heating simultaneously. Joule heating is the heat generated whenever a current passes through a resistive material [8]. The thermal performance of a hybrid PVT collector is also likely to be affected by Joule heating [9], [10]. Joule heating effect exists when the hybrid PVT collector generates electrical and thermal energy as PVT-mode [11].

PV module temperature is more determined through prediction. It used data from the manufacturer as environmental data (irradiation, ambient air temperature, wind speed). Moreover, the prediction data only used electrical parameters provided by the PV manufacturers [12]–[15]. If the prediction of PV module temperature is too low, then the actual efficiency of PV modules is often lower than the PV manufacturer data by standard test conditions (STC: 1000 W/m², 25 °C, AM 1.5). There have been several methods and techniques in predicting PV temperature. Direct measurement by attaching a thermocouple to the solar cell from the back-sheet can accurately predict the PV temperature [16]. However, the temperature sensor insertion into a PV cell is quite challenging. The nominal operating cell temperature (NOCT) model is more accurate in predicting the PV temperature for the PVT system [17]. However, these models also depend on the accuracy of the environmental and operational data. Artificial intelligence (AI) techniques with artificial neural network (ANN) [18]–[20], modelling with various models [21]–[23] are satisfactory in estimating the PV module temperature. However, all these techniques have not demonstrated the physics interaction of input parameters, such as environmental and operational data. A model to estimate PV temperature involving wind speed effects gives quite reliable results [24]–[26]. However, the model is very dependent on the availability of wind speed data, in addition to data storage memory. Estimating the radiation and module temperature have used the algebra equation and non-linear parameter techniques [27]. The PV system must be on maximum power point tracking (MPPT). However, these methods require certainty data with quite complex calculations. In addition, Joule heating were not involved in the discussion.

Joule heating has difficulty observing outdoors for a long measurement. Joule heating requires the ideal conditions such as; high irradiation, long duration of the steady conditions and slight temperature differences between inlet water and ambient air. The system must be in a steady state to be more controlled for getting an accurate result. While most of the indoor ones only used a small PV cell, it was not easy to detect and measure Joule heating. Thus, several studies have examined Joule heating by simulation rather than experimentation. A finite element model using COMSOL Multiphysics simulated the PV module temperature and Joule heating [28]. The PV module temperature was corrected using simulation for a constant current density. However, Joule heating was neglected for more complex simulations reasoning less contribution comparing irradiances and memory concerns. The comprehensive energy distribution model [29], the novel thermal model [30] also the electrical loss prediction of modules (ELMO), and the outdoor measurement method [31] investigated the electrical and thermal performance of PV modules including the series resistance loss from Joule heating. The model determined the amount of incident solar energy lost. However, there was no detailed discussion regarding Joule heating. The heat transfer model was developed based on the ambient condition [32]. It can implicitly involve the Joule heating in the simulation. Unfortunately, Joule heating has not been the main focus to examine in more detail. Finally, Joule heating did not involve in the model development. The 1D numerical model predicted the cell efficiency and temperature during operation [33]. This model encompassed every heat mechanism occurring in a solar cell.

Research on the system performance of PV or PVT modules through module temperature is still quite interesting especially involving Joule heating. From previous studies, it seems that there have been some researches that specifically discuss the behaviour of PV or PVT module temperature as an effect of Joule heating. Although all studies have examined the PV module temperature, electrical and thermal efficiency; however, Joule heating has not been explicitly discussed [32]. The experiments could observe Joule heating but neglected it due to simplifying formulation. For continuing the previous study [34], the present work is to validate the Joule heating experimentally by investigating the thermal distribution of PV cells under PV-On or generating electricity and PV-Off or without generating electricity. The current study purposes in estimating the value of Joule heating which affected the PV module temperature during PV-On.

2. METHOD

2.1. Experimental setup

Since the ideal conditions are hardly difficult to achieve outdoors, the experiments have been done indoors. Figure 1 shows the indoor experimental configuration using a halogen solar simulator. The halogen solar simulator can control the significant parameters properly. The comprehensive dimensions, designs, and characteristics of the simulator were previously discussed [35]. Before the experiment, the irradiance level was adjusted by the sliding regulator (Matsunaga, SD-1310) to the simulator and measured by a pyranometer (MS-42, Eko) at the midpoint of the PV module mounting surface (mc-Si, GT434 type, KIS Solar Japan). Then, the PV module changed the pyranometer position, connected to the simulator [35], sliding variable resistor (Berco, Rheostats), and analogue-digital-converter (ADC). The sliding variable resistor R_{mpp} adjusted the MPPT [36], [37]. The ADC (WE1C, Fuji electric) accumulated and converted the electrical data, such as voltage [V], ampere [A], and power [W]. The PV cell temperature $T_{pv(1-8)}$ from the T-type thermocouple connected to the

data logger (GL220, 10 channels, Graphtec) with a 30 s sampling time. The room temperature T_r as the ambient air temperature T_a was set to 25 °C and recorded by the thermograph.

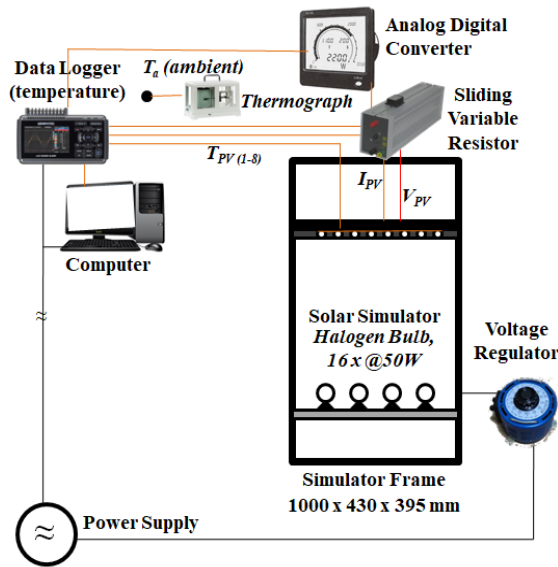


Figure 1. Indoor experimental configuration

2.2. Detailed measurement position

Figure 2 shows the detailed measurement position of the PV module. Figure 2(a) shows the PV cells coordinate at the rear surface to measure the temperature of each cell. As shown, there are four rows, each row with eight cells. The outer dimension of the PV module is 380x350 mm, giving the total area A_{pv} is 0.133 m². The PV module had 17 cells with 35×160 mm for each cell. Each cell gave an effective area of about 0.0054 m². The total area of the PV cells A_{si} was 0.091 m² or approximately 69% of the total area of the PV module A_{pv} . Figure 2(b) describes the coordinate position of the halogen light sources. As a reference, the lower-left corner was the centre (0.0). The previous studies have discussed the detailed dimensions, construction, and characteristics of the solar simulator and the PV module [27]–[29]. Table 1 shows the specific measurement positions.

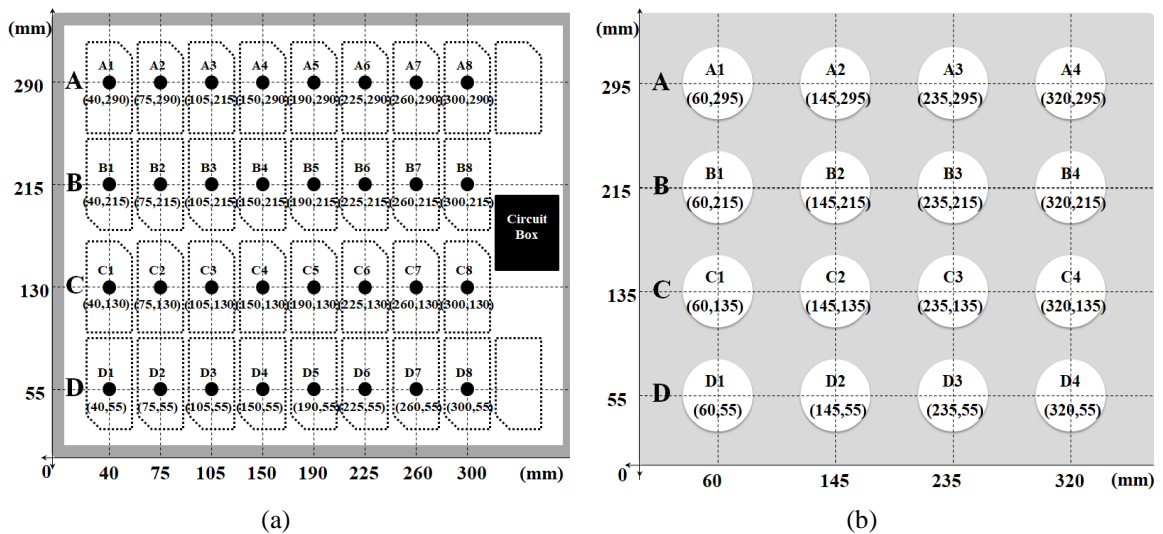


Figure 2. Detailed measurement: (a) PV cells coordinate and (b) reference position with halogen bulbs

Table 1. Summary coordinate position of PV cells and halogen bulbs

Row	Cells Position in PV Module								Halogen Position in Solar Simulator			
	1	2	3	4	5	6	7	8	1	2	3	4
A	(40;290)	(75;290)	(105;290)	(150;290)	(190;290)	(225;290)	(260;290)	(300;290)	(60;295)	(145;295)	(235;295)	(320;295)
B	(40;215)	(75;215)	(105;215)	(150;215)	(190;215)	(225;215)	(260;215)	(300;215)	(60;215)	(145;215)	(235;215)	(320;215)
C	(40;130)	(75;130)	(105;130)	(150;130)	(190;130)	(225;130)	(260;130)	(300;130)	(60;135)	(145;135)	(235;135)	(320;135)
D	(40;55)	(75;55)	(105;55)	(150;55)	(190;55)	(225;55)	(260;55)	(300;55)	(60;55)	(145;55)	(235;55)	(320;55)

2.3. Measurement and data collection

For the study purpose, an experiment on the PV module temperature had conducted during PV-On and PV-Off. That is to determine the difference in temperature distribution between PV-On and PV-Off due to the Joule heating on the PV module. The measurement of each cell temperature took the rear surface of the PV module. This method allowed the light to reach the PV cell surface without being blocked by thermocouples. As a benchmark, measurement took 32 points. The steady-state measurements were made during MPPT with $R_{mpp} \approx 30; 33; 37; 41 \Omega$ for the fixed irradiances $I=1000; 900; 800; 700 \text{ W/m}^2$, respectively. Due to the limited data-logger ports (only ten ports), measurements were made row by row, with the same conditions and treatment for each row. An experiment used eight ports to measure the temperature of each cell, the remaining two more ports for voltage V_{pv} and power P_{pv} of the PV module. The experiment started from row A with $I = 1000 \text{ W/m}^2$. For measurement stability and accuracy, each endpoint of the T-thermocouple was given a speck of wax and affixed to the measurement point, then covered with a thin transparent tape. First, turn on the simulator. Then, connected the circuit for PV-On. After 30-40 minutes, the system reached the steady-state. With 1-minute intervals, measuring 3 data were taken for stability. Then, the circuit was cut off for PV-Off without turning off the simulator lights and left for about 10 minutes before repeating the same measurement. The same treatment and conditions repeated the experiments for rows B, C, D during PV-On and PV-Off for $I=900; 800; 700 \text{ W/m}^2$. Table 2 shows the summaries of measurement and data collections.

Table 2. Summary of measurement and data collections

Exp.	Row (see Figure 2)	Points (see Figure 2)	Activities (minutes)					Irradiances (W/m^2)	
			0-40	40-45	46-55	55-60	60-90		
1	A	8	$A_n (n = 1, 2, 3, \dots, 8)$	Steady	3 data	Steady	3 data	cooling	$1000 \rightarrow 900 \rightarrow 800 \rightarrow 700$
2	B	8	$B_n (n = 1, 2, 3, \dots, 8)$	Steady	3 data	Steady	3 data	cooling	$1000 \rightarrow 900 \rightarrow 800 \rightarrow 700$
3	C	8	$C_n (n = 1, 2, 3, \dots, 8)$	Steady	3 data	Steady	3 data	cooling	$1000 \rightarrow 900 \rightarrow 800 \rightarrow 700$
4	D	8	$D_n (n = 1, 2, 3, \dots, 8)$	Steady	3 data	Steady	3 data	cooling	$1000 \rightarrow 900 \rightarrow 800 \rightarrow 700$

2.4. Theoretical and practical calculation

As assumed previously, the effect of Joule heating resulted in a rising in temperature. The investigation of Joule heating needs to carry on during PV-On vs PV-Off. To illustrate the different temperature distributions of PV-On and PV-Off, a normal probability density function (NPDF) of each PV cell temperature $T_{pv,n}$ in Gaussian distributions formulated as [38]:

$$NPDF = f(T_{pv,n}) = \frac{1}{\sqrt{2\pi}\sigma} e^{-\frac{(T_{pv,n}-\mu)^2}{2\sigma^2}} \quad (1)$$

where; μ , π and σ are the mean, the constant number, and the standard deviation of the PV cell temperatures distribution, respectively, while subscript n is cells 1 to 32. The *NPDF* can be proceeded using the Excel syntax function: NORMDIST (x, mean, standard_dev, false) [39].

The electrical efficiency η_e as the dependent of the PV temperature T_{pv} is expressed in [3], [4]:

$$\eta_e = \eta_o [1 - 0.0045(T_{pv} - 25)] \quad (2)$$

where; η_o is the efficiency of the PV module (STC). For every $1 \text{ }^\circ\text{C}$ increase of T_{pv} at STC as in (2), then η_e will decrease by 0.0045. It is due to increased recombination losses of PV cells [29]. Practically, the electrical efficiency η_e is also given [40];

$$\eta_e = \frac{V_{pv} I_{pv}}{A_{pv} I} \quad (3)$$

where; V_{pv} , I_{pv} and A_{pv} indicate as the voltage [V], the current [A] with a specific load applied [Ω] to a PV module area [m^2], respectively. The heat sources for the PV module have been identified as solar irradiance and Joule's heating effect [32]. Joule heating as internal heating Q_{jh} [W] linearly dependent on the internal series resistance R_{si} [Ω], but dependence quadratically on the current-induced I_{pv} [29];

$$Q_{ih} = I_{pv}^2 R_{si} \tag{4}$$

Figure 3 shows the Joule heating conduction model from layer to layer. For simplification, assume; a). The system was in a steady-state with heat transfer only affected by Joule heating [41]. b). Silicon layer as a source of Joule heating [32], c). No Joule heating absorbed by the frame due to silicon packing, d). No loss by convection for Joule heating, e). PV layer temperature was the same for each point. As shown in Figure 3(a), the Q_{jh} can be estimated during PV-On vs PV-Off;

$$Q_{jh} = (m_{gl}c_{p,gl} + m_{eva}c_{p,eva} + m_{si}c_{p,si} + m_{eva}c_{p,eva} + m_{tpt}c_{p,tpt})\Delta T_{pv} \tag{5}$$

where; m and c_p are the mass [g] and specific heat [J/g. $^{\circ}C$] of the individual layer. The subscript gl , eva , si , tpt are the glass, eva (ethylene vinyl acetate), silicon, and tedlar/polyester/tedlar, respectively, as shown in Table 3. Then, ΔT_{pv} [$^{\circ}C$] is the temperature difference between PV-On and PV-Off.

From (5) and Figure 3, Joule heating Q_{ih} can be formulated as (6),

$$Q_{jh} = (k_{si} \frac{A_{si} \Delta T_{pv}}{2 L_{si}} + k_{eva} A_{eva} \frac{\Delta T_{pv}}{L_{eva}} + k_{gl} A_{gl} \frac{\Delta T_{pv}}{L_{gl}}) + (k_{si} \frac{A_{si} \Delta T_{pv}}{2 L_{si}} + k_{eva} A_{eva} \frac{\Delta T_{pv}}{L_{eva}} + k_{tpt} A_{gl} \frac{\Delta T_{pv}}{L_{tpt}}) \tag{6}$$

where; k , A and L are the thermal conductivity [W/m. $^{\circ}C$], the area [m^2] and the thickness [m] of the individual layer, then the subscript gl , eva , si , tpt are the glass, eva (ethylene vinyl acetate), silicon, and tedlar/polyester/tedlar, respectively. To estimate the overall thermal conductivity k_{pv} simplifying as (7);

$$Q_{jh} = k_{pv} A_{pv} \frac{\Delta T_{pv}}{L_{pv}} \quad or, \quad Q_{jh} = \frac{\Delta T_{pv}}{R_{pv}} \tag{7}$$

where; A_{pv} [m^2] and L_{pv} [m] are the total areas and total thickness of the PV module. Then, $L_{pv}/k_{pv}A_{pv}$ is the overall thermal resistance R_{pv} [$^{\circ}C/W$] as shown in Figure 3 (b). Table 3 shows the material properties of the PV module required by the formula above; thermal conductivity k [W/m. $^{\circ}C$], specific heat c_p [J/kg. $^{\circ}C$], specific density ρ [kg/ m^3], thickness L [m], as well as the estimated mass m [kg] and volume V [m^3].

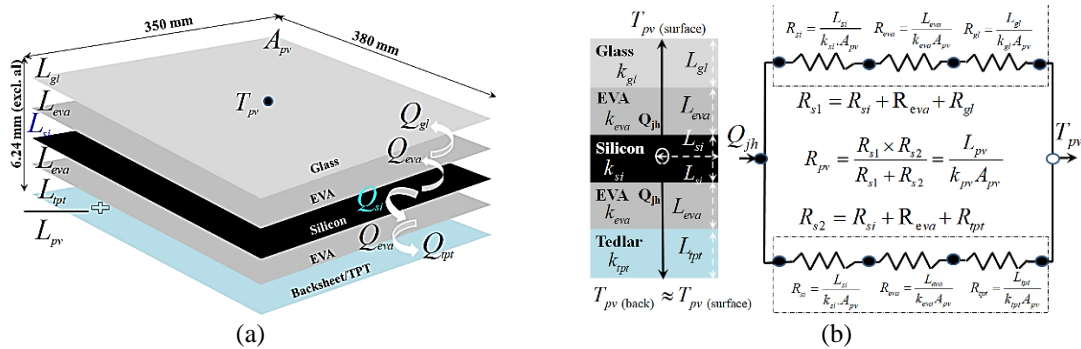


Figure 3. Joule heating conduction model: (a) layer to layer conduction and (b) thermal description

Table 3. Material properties of the PV layers (summarized and estimated from [32], [40], [42])

Layer/Material (subscript)	Conductivity k [W/m. $^{\circ}C$]	Specific heat c_p [J/kg. $^{\circ}C$]	Specific density ρ [kg/ m^3]	Thickness L [m]	Mass m [kg]	Volume V [m^3]
Top cover/Glass (gl)	1.04	8.40×10^2	2.5×10^3	2.50×10^{-3}	0.404×10^{-3}	3.20×10^2
Encapsulant/EVA (eva)	0.29	2.90×10^3	9.6×10^3	0.50×10^{-3}	0.031×10^{-3}	0.65×10^2
PV cell/Silicon (si)	142.00	6.77×10^2	2.3×10^3	0.24×10^{-3}	0.056×10^{-3}	0.61×10^2
Encapsulant/EVA (eva)	0.29	2.90×10^3	9.6×10^3	0.50×10^{-3}	0.031×10^{-3}	0.65×10^2
Backsheet/TPT (tpt)	0.14	1.25×10^3	1.2×10^3	2.50×10^{-3}	0.404×10^{-3}	3.20×10^2
Total				6.24×10^{-3}	1.906×10^{-3}	8.31×10^2

3. RESULTS AND DISCUSSION

Figure 4 demonstrates the PV surface temperature T_{pv} and electrical efficiency η_e from starting to reach a steady-state. As shown, the room temperature T_r was relatively stable with an average of 25.3 °C. Each irradiance I had a different T_{pv} increased, where an increase in I gave a faster T_{pv} rise. The fastest T_{pv} rise occurred in the collection-state (0-15 minutes) when the mass begins to collect heat, then enters the transition-state (15-30 minutes) starting to slow down and eventually flattens out into a steady-state (after 30 minutes). The effect of increasing T_{pv} causing a decrease in η_e (2). In the collection-state, η_e decreased faster with higher T_{pv} , due to higher I . After reaching a steady-state, η_e has tended to be stable.

Figure 5 shows the bell-shaped curves normal distribution of T_{pv} during steady-state for PV-On and PV-Off. The curves are constructed based on each cell temperature with fixed irradiance I in (1), Figures 5(a) to 5(d) represent $I=1000, 900, 800, 700$ W/m², respectively. As shown in Figures 5(a) to 5(d), the mean T_{pv} increased with increasing I . The graphs show that the difference in the temperature distribution of each cell decreased with decreasing I . As shown, the T_{pv} distribution got closer to the mean temperature. The normal distribution curve will be higher. However, the difference between T_{pv} for PV-On and PV-Off diminished as I decreased.

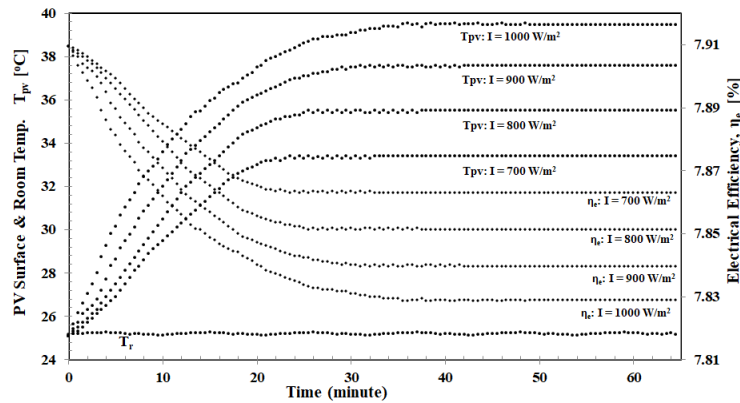


Figure 4. Measuring data to steady-state; PV surface temp. vs time, and electrical efficiency vs time

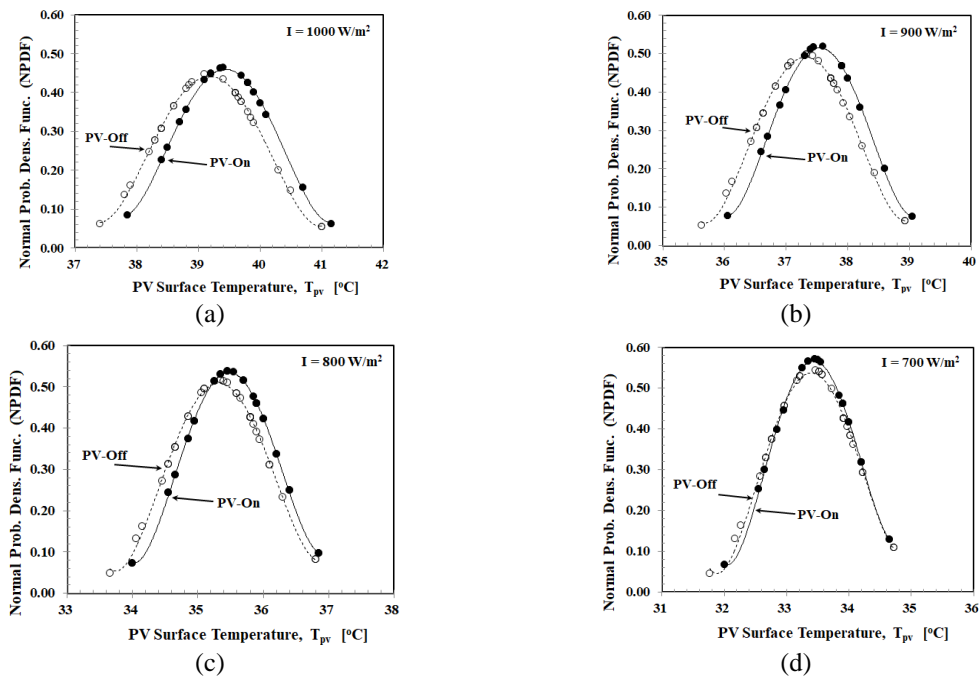


Figure 5. Distribution of T_{pv} : (a) $I=1000$ W/m², (b) $I=900$ W/m², (c) $I=800$ W/m², and (d) $I=700$ W/m²

Figure 6 shows the thermal and electrical performance during steady-state. The relationship between PV surface temperature T_{pv} and irradiance I under PV-On and PV-Off conditions is given in Figure 6(a). As shown, the T_{pv} increased with increasing I or vice versa. The difference between T_{pv} for PV-On and PV-Off was greater with increasing irradiance, and close to zero for $I \approx 620 \text{ W/m}^2$. Figure 6(b) shows the relationship between electrical efficiency η_e for PV-On with PV module temperature T_{pv} . As shown, the η_e decreased with increasing T_{pv} , or vice versa. From the graph, the temperature efficiency coefficient $\mu = -0.0049/^\circ\text{C}$ is quite reasonable compared to the previous studies [3], [42], [43].

The complete results for PV surface temperature T_{pv} , standard deviation σ , root mean square error ϵ and Joule heating Q_{ih} are summarized in Table 4. As shown, the irradiance decreased so that T_{pv} , σ , ϵ , Q_{ih} also decreased. Table 5 compares the present and previous results [32], such as thermal resistance R_{pv} and temperature rise due to current (Joule heating) $\Delta T_{pv}/I_{pv}$. The lower thermal resistance R_{pv} in the current result compared to the previous result was probably due to the different PV module construction. However, the temperature rise due to the current $\Delta T_{pv}/I_{pv}$ was not much different.

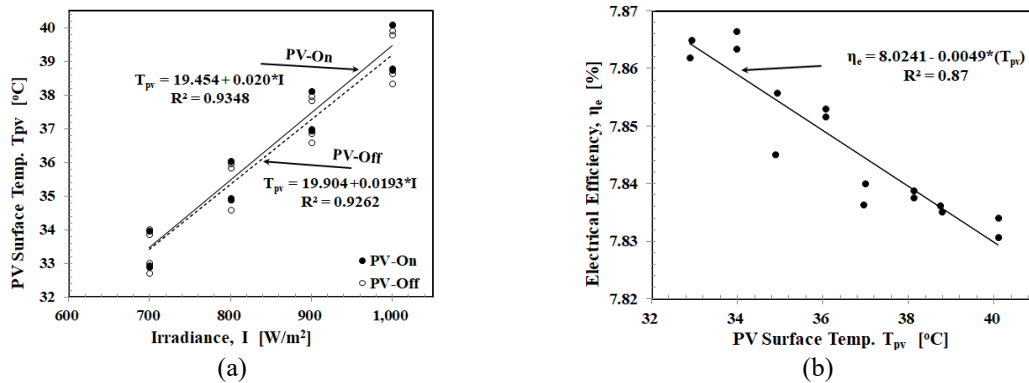


Figure 6. PV performance: (a) PV surface temp. vs irradiance, and (b) elect. efficiency vs PV temp.

Table 4. Summary results of PV-On vs PV-Off

Items	I = 1000 W/m ²		I = 900 W/m ²		I = 800 W/m ²		I = 700 W/m ²		
	PV-On	PV-Off	PV-On	PV-Off	PV-On	PV-Off	PV-On	PV-Off	
PV surface temperature	T_{pv} [°C]	39.43	39.17	37.52	37.33	35.48	35.37	33.44	33.41
Std. Deviation	σ [°C]	0.86	0.89	0.77	0.81	0.74	0.77	0.70	0.71
Root Mean Sq. error	ϵ [°C]	0.84	0.88	0.76	0.79	0.73	0.76	0.69	0.70
Joule heating (calculated)	Q_{ih} [J]	842.52	-	744.78	-	515.72	-	123.57	-

Table 5. Comparison to the closely related previous result [29], [32]

Items	Result Comparison		
	Proposed	Ying [32]	
Thermal resistance in (8), R_{pv}	m ² .K/W	0.0049	0.0041–0.0043
Temp. rise due to current (Joule heating) $\Delta T_{pv}/I_{pv}$	K/A	0.53	0.54

From the results with the condition of PV-On and PV-Off, such as; normal distribution, mean of T_{pv} , ΔT_{pv} , thermal and electrical performance, and so on, three things can be discussed. First, related to the thermal distribution from Figure 5. The reason why the distribution of PV module temperature follows the normal curve is that follows the irradiance uniformity pattern of the simulator [35]. The detailed overlap coordinate position between halogen light sources and the PV module has shown in Figure 2. There was a slight $\leq 0.3 \text{ }^\circ\text{C}$ of the temperature difference ΔT_{pv} between PV-On and PV-Off. The small ΔT_{pv} may be caused by the small I_{pv} generated by the small A_{pv} . For $I = 1000 \text{ W/m}^2$, the difference T_{pv} in the middle and at the edge was $2 \text{ }^\circ\text{C}$. The temperature rise due to the current $\Delta T_{pv}/I_{pv}$ was 0.53 K/A . Those are close to the glass to back sheet (GB) module [32]. Implicitly, it might be due to irradiance as well as Joule heating [9], [10].

Second, related to the thermal and electrical performance of the PV module as shown in Figure 6. The temperature uniformity of PV cells is one of the main factors affecting electrical efficiency. With a more uniform temperature distribution, the electrical efficiency will be higher (2). The output power will be even

greater. Conversely, the PV module temperature increases, the power output will decrease. As a result, the fill factor (FF) decreased, which mean the electrical efficiency of PV also decreases [44].

Third, related to the overall thermal conductivity k_{pv} and thermal resistance R_{pv} . Referring to Figures 3(a) and 3(b) at steady-state and constant ambient air temperature T_a , the k_{pv} changes with load variations R_{mpp} . With fixed A_{pv} and L_{pv} , when I increases, causing ΔT_{pv} to increase, then Q_{jh} also increases. In this case, the Joule heating might slightly increase k_{pv} and also slightly decrease R_{pv} (from glass cover to back sheet) which affect the heat transfer [32]. The difference in operational temperature of each PV cell results in different performance. The PV module accuracy decreases from low-temperature toward the high-temperature range [45].

Finally, the effect of Joule heating has been proved and estimated, with the results positively correlated to the irradiances increase from 700-1000 W/m². For more accurate results, further experiments use more precise and sophisticated instrumentation. This study tries to estimate the effect of Joule heating in a PV module as a reference analysis for PV and PVT performances. The current study contributes to improving the procedure of predicting PV module temperature by considering the Joule heating. In practical application, Joule heating optimises the electrical efficiency of PV modules. Joule heating also increases the thermal and electrical performance of the PVT system as additional heat [9], [10], [15]. By involving the temperature distribution of each PV cell, the performance prediction and calculation of PV or PVT module temperature will be more accurate. For future research, the performance of a large PV or PVT system should consider Joule heating as a complement by improving the performance modelling tools, system design and development [46]–[48].

4. CONCLUSION

The existence of Joule heating has been investigated indoors by comparing the PV surface temperature of each cell with the higher irradiances of 700-1000 W/m² during PV-On and PV-Off in steady-state. The PV module temperature distribution follows the curve as the irradiation uniformity pattern of the solar simulator with a slight ≤ 0.3 °C difference between PV-On and PV-Off. Joule heating slightly increased the PV module temperature of 0.53 °C/A, which is proportional to the irradiances. Joule heating has increased almost seven times from 2.65 W at 700 W/m² to 18.07 W at 1000 W/m². Joule heating might slightly increase the overall thermal conductivity and also slightly decrease the thermal resistance. Joule heating affects heat transfer. For more accurate results, further experiments use more precise and sophisticated instrumentation. This research may improve the procedure in predicting the PV module temperature by considering the Joule heating during the PV-On and also PVT-mode. Joule heating increases the electrical efficiency of the PV module and the thermal efficiency of the PVT collector. For future research, consider Joule heating in the thermal and electrical performance of a large PV module or PVT collector by improving the modelling and control systems.

ACKNOWLEDGEMENTS

A part of this work was done and supported by the “High-Tech Research Project” for Private Universities through a matching fund subsidy from the Ministry of Education, Culture, Sports, Science and Technology, Japan, the grant number 07H018. Thanks to; Dr. Mika Yoshinaga from Meijo University, Nagoya, Japan, Prof. Takeshi Kawashima and Prof. Kazutaka Itako from Kanagawa Institute of Technology on the research opportunity and discussion, to Prof. TMI Mahlia from the University of Technology Sydney, Prof. Rinaldi Idroes from Syiah Kuala University and Dr. Sparisoma Viridi from Bandung Institute of Technology for their valuable support.

REFERENCES

- [1] M. A. Green, Y. Hishikawa, E. D. Dunlop, D. H. Levi, J. Hohl-Ebinger, and A. W. Y. Ho-Baillie, “Solar cell efficiency tables (version 52),” *Prog. Photovoltaics Res. Appl.*, vol. 26, no. 7, pp. 427–436, 2018, doi:10.1002/pp.3040.
- [2] N. Akram *et al.*, “A comprehensive review on nanofluid operated solar flat plate collectors,” *J. Therm. Anal. Calorim.*, vol. 139, no. 2, pp. 1309–1343, 2020, doi:10.1007/s10973-019-08514-z.
- [3] A. Tarabsheh Al *et al.*, “Performance of photovoltaic cells in photovoltaic thermal (PVT) modules,” *IET Renew. Power Gener.*, vol. 10, no. 7, pp. 1017–1023, 2016, doi:10.1049/iet-rpg.2016.0001.
- [4] I. Guarracino, J. Freeman, A. Ramos, S. A. Kalogirou, N. J. Ekins-daukes, and C. N. Markides, “Systematic testing of hybrid PV-Thermal (PVT) solar collectors in steady-state and dynamic outdoor conditions,” *Appl. Energy*, vol. 240, no. December 2018, pp. 1014–1030, 2019, doi:10.1016/j.apenergy.2018.12.049.
- [5] I. Etier, S. Nijmeh, M. Shdiefat, and O. Al-Obaidy, “Experimentally evaluating electrical outputs of a pv-t system in jordan,” *Int. J. Power Electron. Drive Syst.*, vol. 12, no. 1, pp. 421–430, 2021, doi:10.11591/ijpeds.v12.i1.pp421-430.
- [6] A. Herez, H. El, T. Lemenand, and M. Ramadan, “Review on photovoltaic/thermal hybrid solar collectors: Classifications, applications and new systems,” *Sol. Energy*, vol. 207, no. February, pp. 1321–1347, 2020, doi:10.1016/j.solener.2020.07.062.
- [7] A. Fudholi and K. Sopian, “R&D of Photovoltaic Thermal (PVT) Systems: an Overview,” *Int. J. Power Electron. Drive Syst.*, vol. 9, no. 2, p. 803, 2018, doi:10.11591/ijpeds.v9.i2.pp803-810.
- [8] A. Khatibi, F. Razi Astaraei, and M. H. Ahmadi, “Generation and combination of the solar cells: A current model review,” *Energy*

- Sci. Eng.*, vol. 7, no. 2, pp. 305–322, 2019, doi:10.1002/ese3.292.
- [9] E. Yandri, “The Effect of Joule Heating to Thermal Performance of hybrid PVT Collector during Electricity Generation,” *Renew. Energy*, vol. Volume 111, no. October 2017, p. Pages 344–352, 2017, doi:10.1016/j.renene.2017.03.094.
- [10] H. Yoshida, S. Daidouji, K. Itako, and N. Hagino, “Thermal Behavior of Photovoltaic-Thermal Hybrid Collector,” in *Proceedings of EuroSun2016*, 2016, no. October, pp. 1–11. doi:10.18086/eurosun.2016.08.17.
- [11] J. Appelbaum and T. Maor, “Dependence of pv module temperature on incident time-dependent solar spectrum,” *Appl. Sci.*, vol. 10, no. 3, 2020, doi:10.3390/app10030914.
- [12] A. Senturk and R. Eke, “A new method to simulate photovoltaic performance of crystalline silicon photovoltaic modules based on datasheet values,” *Renew. Energy*, vol. 103, pp. 58–69, 2017, doi:10.1016/j.renene.2016.11.025.
- [13] N. Bouaziz, A. Benfdila, and A. Lakhlef, “A model for predicting photovoltaic module performances,” *Int. J. Power Electron. Drive Syst.*, vol. 10, no. 4, pp. 1914–1922, 2019, doi:10.11591/ijpeds.v10.i4.1914-1922.
- [14] K. H. Hassan, A. T. Rashid, and B. H. Jasim, “Parameters estimation of solar photovoltaic module using camel behavior search algorithm,” *Int. J. Electr. Comput. Eng.*, vol. 11, no. 1, pp. 788–793, 2021, doi:10.11591/ijece.v11i1.pp788-793.
- [15] M. S. Ismail, M. Moghavvemi, and T. M. I. Mahlia, “Characterization of PV panel and global optimization of its model parameters using genetic algorithm,” *Energy Convers. Manag.*, vol. 73, pp. 10–25, 2013, doi:10.1016/j.enconman.2013.03.033.
- [16] K. Nishioka, K. Miyamura, Y. Ota, M. Akitomi, Y. Chiba, and A. Masuda, “Accurate measurement and estimation of solar cell temperature in photovoltaic module operating in real environmental conditions,” *Jpn. J. Appl. Phys.*, vol. 57, no. 8, pp. 1–5, 2018, doi:10.7567/JJAP.57.08RG08.
- [17] V. Sun, A. Asanakhm, T. Deethayat, and T. Kiatsiriroat, “A new method for evaluating nominal operating cell temperature (NOCT) of unglazed photovoltaic thermal module,” *Energy Reports*, vol. 6, pp. 1029–1042, 2020, doi:10.1016/j.egy.2020.04.026.
- [18] O. May Tzuc, A. Bassam, P. E. Mendez-Monroy, and I. S. Dominguez, “Estimation of the operating temperature of photovoltaic modules using artificial intelligence techniques and global sensitivity analysis: A comparative approach,” *J. Renew. Sustain. Energy*, vol. 10, no. 3, 2018, doi:10.1063/1.5017520.
- [19] X. Xu *et al.*, “Current characteristics estimation of Si PV modules based on artificial neural network modeling,” *Materials (Basel)*, vol. 12, no. 18, pp. 1–12, 2019, doi:10.3390/ma12183037.
- [20] A. F. M. Nor, S. Salimin, M. N. Abdullah, and M. N. Ismail, “Application of artificial neural network in sizing a stand-alone photovoltaic system: A review,” *Int. J. Power Electron. Drive Syst.*, vol. 11, no. 1, pp. 342–349, 2020, doi:10.11591/ijpeds.v11.i1.pp342-349.
- [21] C. Coskun, U. Toygar, O. Sarpdag, and Z. Oktay, “Sensitivity analysis of implicit correlations for photovoltaic module temperature: A review,” *J. Clean. Prod.*, vol. 164, pp. 1474–1485, 2017, doi:10.1016/j.jclepro.2017.07.080.
- [22] E. Barykina and A. Hammer, “Modeling of photovoltaic module temperature using Faiman model: Sensitivity analysis for different climates,” *Sol. Energy*, vol. 146, pp. 401–416, 2017, doi:10.1016/j.solener.2017.03.002.
- [23] M. A. E. H. Mohamed, “The linear model of a PV modul,” *Int. J. Power Electron. Drive Syst.*, vol. 8, no. 2, pp. 900–906, 2017, doi:10.11591/ijpeds.v8i2.pp900-906.
- [24] D. Magare, O. Sastry, R. Gupta, B. Bora, Y. Singh, and H. Mohammed, “Wind Effect Modeling and Analysis for Estimation of Photovoltaic Module Temperature,” *J. Sol. Energy Eng. Trans. ASME*, vol. 140, no. 1, 2018, doi:10.1115/1.4038590.
- [25] M. Akhsassi *et al.*, “Experimental investigation and modeling of the thermal behavior of a solar PV module,” *Sol. Energy Mater. Sol. Cells*, vol. 180, no. March 2017, pp. 271–279, 2018, doi:10.1016/j.solmat.2017.06.052.
- [26] C. Correa-Betanzo, H. Calleja, and S. De León-Aldaco, “Module temperature models assessment of photovoltaic seasonal energy yield,” *Sustain. Energy Technol. Assessments*, vol. 27, no. June 2017, pp. 9–16, 2018, doi:10.1016/j.seta.2018.03.005.
- [27] E. Moshksar and T. Ghanbari, “Real-time estimation of solar irradiance and module temperature from maximum power point condition,” *IET Sci. Meas. Technol.*, vol. 12, no. 6, pp. 807–815, 2018, doi:10.1049/iet-smt.2017.0476.
- [28] N. Peter, O. E. Kabu, K. Stephen, and D. Anthony, “3D Finite Element Method Modeling And Simulation Of The Temperature Of Crystalline Photovoltaic Module,” *Int. J. Res. Eng. Technol.*, vol. 04, no. 09, pp. 378–384, doi:10.15623/ijret.2015.0409070.
- [29] L. Shen, Z. Li, and T. Ma, “Analysis of the power loss and quantification of the energy distribution in PV module,” *Appl. Energy*, vol. 260, no. December 2019, 2020, doi:10.1016/j.apenergy.2019.114333.
- [30] A. K. Abdulrazzaq, B. Plesz, and G. Bognár, “A novel method for thermal modelling of photovoltaic modules/cells under varying environmental conditions,” *Energies*, vol. 13, no. 13, 2020, doi:10.3390/en13133318.
- [31] G. Spagnuolo, K. Lappalainen, S. Valkealahti, and P. Manganiello, “Identification and diagnosis of a photovoltaic module based on outdoor measurements,” *2019 IEEE Milan PowerTech, PowerTech 2019*, 2019, doi:10.1109/PTC.2019.8810767.
- [32] D. Ying, W. Tao, Y. Liu, J. Jiang, and H. Huang, “Heat transfer modeling and temperature experiments of crystalline silicon photovoltaic modules,” *Sol. Energy*, vol. 146, no. April 2017, pp. 257–263, 2017, doi:https://doi.org/10.1016/j.solener.2017.02.049
- [33] R. Couderc, M. Amara, and M. Lemiti, “In-Depth Analysis of Heat Generation in Silicon Solar Cells,” *IEEE J. Photovoltaics*, vol. 6, no. 5, pp. 1123–1131, 2016, doi:10.1109/JPHOTOV.2016.2566923.
- [34] E. Yandri, “Dataset of the PV surface temperature distribution when generating electricity (PV-On) and without generating electricity (PV-Off) using Halogen Solar Simulator,” *Data Br.*, vol. 27, p. 104578, 2019, doi:10.1016/j.dib.2019.104578.
- [35] E. Yandri, “Uniformity characteristic and calibration of simple low cost compact halogen solar simulator for indoor experiments,” *Int. J. Low-Carbon Technol.*, no. May, pp. 1–13, 2018, doi:10.1093/ijlct/cty018.
- [36] A. A. Abdulrazzaq and A. H. Ali, “Efficiency performances of two MPPT algorithms for PV system with different solar panels irradiances,” *Int. J. Power Electron. Drive Syst.*, vol. 9, no. 4, pp. 1755–1764, 2018, doi:10.11591/ijpeds.v9.i4.pp1755-1764.
- [37] H. Attia and K. Hossin, “Hybrid technique for an efficient PV system through intelligent MPPT and water cooling process,” *Int. J. Power Electron. Drive Syst.*, vol. 11, no. 4, p. 1835, Dec. 2020, doi:10.11591/ijpeds.v11.i4.pp1835-1843.
- [38] Y. Zhang, Z. Jin, and S. Mirjalili, “Generalized normal distribution optimization and its applications in parameter extraction of photovoltaic models,” *Energy Convers. Manag.*, vol. 224, no. August, p. 113301, 2020, doi:10.1016/j.enconman.2020.113301.
- [39] O. Support, “Excel for the web - NORM.DIST function,” *Microsoft*, 2019. <https://support.microsoft.com/en-us/office/norm-dist-function-edb1cc14-a21c-4e53-839d-8082074c9f8d>.
- [40] E. Yandri, “Development and experiment on the performance of polymeric hybrid Photovoltaic Thermal (PVT) collector with halogen solar simulator,” *Sol. Energy Mater. Sol. Cells*, vol. 201, no. December 2018, p. 110066, 2019, doi:10.1016/j.solmat.2019.110066.
- [41] A. İ. A. İlhan CEYLAN, Sezayi YILMAZ, Özgür İNANÇ, Alper ERGÜN, Ali Etem GÜREL, Bahadır ACAR, “Determination of the heat transfer coefficient of pv panels,” *Energy*, 2019, doi:10.1016/j.energy.2019.03.152.
- [42] S. Kaplanis and E. Kaplani, “A New Dynamic Model to Predict Transient and Steady State PV Temperatures Taking into Account,” *Energies*, vol. 12, no. 2, 2019, doi:10.3390/en12010002.
- [43] N. Kim, D. Kim, H. Kang, and Y. G. Park, “Improved heat dissipation in a crystalline silicon PV module for better performance by using a highly thermal conducting backsheet,” *Energy*, vol. 113, pp. 515–520, 2016, doi:10.1016/j.energy.2016.07.046.

- [44] A. H. Numan, Z. S. Dawood, and H. A. Hussein, "Theoretical and experimental analysis of photovoltaic module characteristics under different partial shading conditions," *Int. J. Power Electron. Drive Syst.*, vol. 11, no. 3, pp. 1508–1518, 2020, doi:10.11591/ijpeds.v11.i3.pp1508-1518.
- [45] H. Mohammed, R. Gupta, O. Sastry, and D. Magare, "Assessment of different correlations to estimate distinct technology PV module operating temperature for Indian site," *Energy Sci. Eng.*, vol. 7, no. 3, pp. 1032–1041, 2019, doi:10.1002/ese3.332.
- [46] A. Lekbir, C. Kim Gan, M. R. Ab Ghani, and T. Sutikno, "The Recovery of Energy from a Hybrid System to Improve the Performance of a Photovoltaic Cell," *Int. J. Power Electron. Drive Syst.*, vol. 9, no. 3, p. 957, 2018, doi:10.11591/ijpeds.v9.i3.pp957-964.
- [47] M. H. Alaaeddin, S. M. Sapuan, M. Y. M. Zuhri, E. S. Zainudin, and F. M. A.- Oqla, "Photovoltaic applications : Status and manufacturing prospects," vol. 102, no. October 2018, pp. 318–332, 2019, doi:10.1016/j.rser.2018.12.026.
- [48] A. H. A. Al-Waeli, H. A. Kazem, M. T. Chaichan, and K. Sopian, "A review of photovoltaic thermal systems: Achievements and applications," *Int. J. Energy Res.*, vol. 45, no. 2, pp. 1269–1308, 2021, doi:10.1002/er.5872.

BIOGRAPHIES OF AUTHORS



Erkata Yandri    graduated in 1994 from Electrical Engineering (Bachelor of Engineering), Universitas Indonesia, Indonesia, and received Master of Renewable Energy (M.Sc.rer.nat) in 2004 from Postgraduate Program Renewable Energy, Universität Oldenburg, Germany. He had experiences working as a solar energy researcher at Kanagawa Institute of Technology, Japan as part of his PhD work. Currently, he works as a researcher/lecturer at the Graduate School of Renewable Energy, Darma Persada University, Indonesia. His current research includes solar photovoltaic, hybrid photovoltaic-thermal (PVT) collector, smart grid, building and industrial energy efficiency, energy-efficient building, energy policy and sustainability. He can be contacted at email: erkata@gmail.com.



Naoto Hagino    received B.S. degree from Kanagawa Institute of Technology, Japan, in 1993 and his M.S. and Ph.D. degrees from Kanagawa Institute of Technology, Japan, in 1995 and 2006, respectively. From 2006 to 2018, he was a part-time lecturer at Kanagawa Institute of Technology, Japan. From 2018 to 2022 was an associate professor at the Department of Comprehensive Engineering, Kindai University Technical College, Japan. Since 2022, he has been an associate professor at the Department of Mechanical Engineering, Faculty of Engineering, Kanagawa Institute of Technology, Japan. His research interests are in fluid dynamics, turbomachinery, metal forming, and thermal engineering. He can be contacted at email: hagino@me.kanagawa-it.ac.jp.